CHEMISTRY
A European Journal

Supporting Information

Supramolecular Photoinduced Electron Transfer between a Redox-Active Hexanuclear Metal–Organic Cylinder and an Encapsulated Ruthenium(II) Complex

Lu Yang, Cheng He,* Xin Liu, Jing Zhang, Hui Sun, and Huimin Guo*[a]

chem_201504975_sm_miscellaneous_information.pdf

Contents

Figure S1 Molecular structure of Ni–**YL** within a unique asymmetric unit.

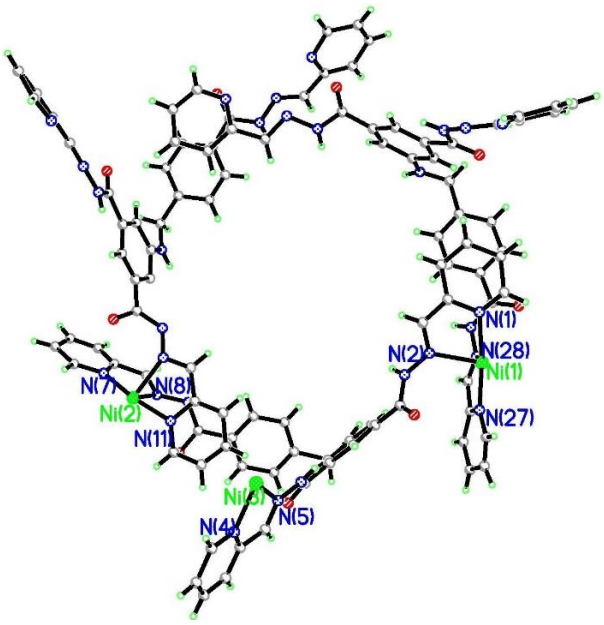

Table S1 Bond distances parameters for Ni and N atoms in a symmetric unit of Ni–**YL**.

Bond	**Bond length**
Ni(1)–N(1)	2.070(6)
Ni(1)–N(2)	2.143(7)
Ni(1)–N(24)#1	2.077(6)
Ni(1)–N(25)#1	2.102(6)
Ni(1)–N(27)	2.051(6)
Ni(1)–N(28)	2.129(6)

Bond	**Bond length**
Ni(2)–N(7)	2.004(6)
Ni(2)–N(8)	2.090(7)
Ni(2)–N(11)	2.098(6)
Ni(2)–N(12)	2.170(6)
Ni(2)–N(14)#1	2.037(6)
Ni(2)–N(15)#1	2.083(6)

Bond	**Bond length**
Ni(3)–N(4)	2.040(6)
Ni(3)–N(5)	2.068(6)
Ni(3)–N(17)#1	2.060(6)
Ni(3)–N(18)#1	2.115(7)
Ni(3)–N(21)#1	2.110(6)
Ni(3)–N(22)#1	2.103(7)

Symmetry code, #1 -x-1,-y-1,z

Figure S2 Representation of Ni–**YL** from top and side views. The tridentate ligand **YL** is represented as tripod in multicolour.

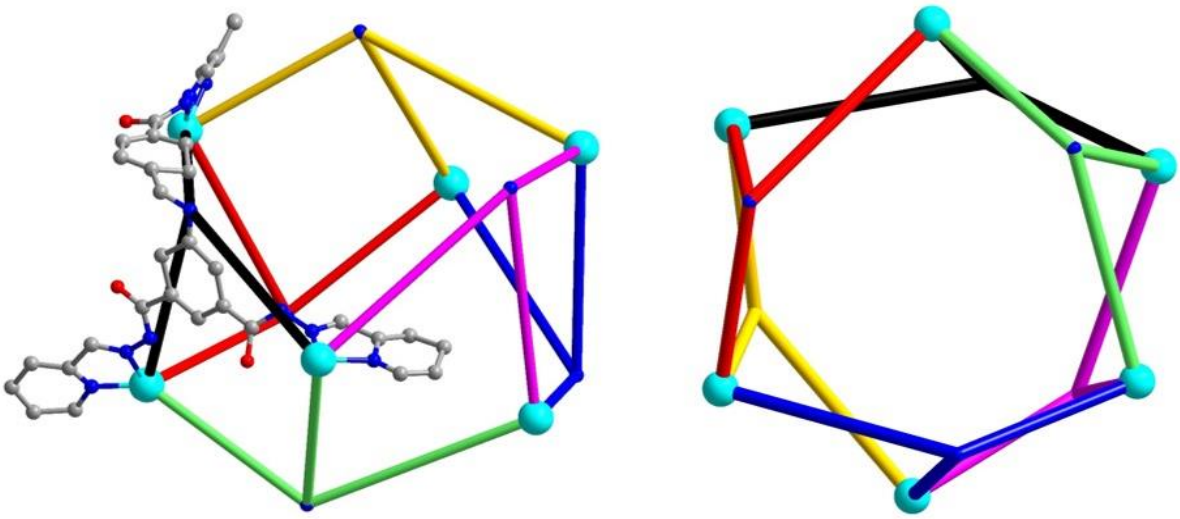

Figure S3 Ball-and-stick structure of Ni–**YL** and the coordination mode of Ni(II) center. Solvent molecules and anions are omitted for clarity. The metal, oxygen, nitrogen and carbon atoms are draw in cyan, red, blue and grey respectively.

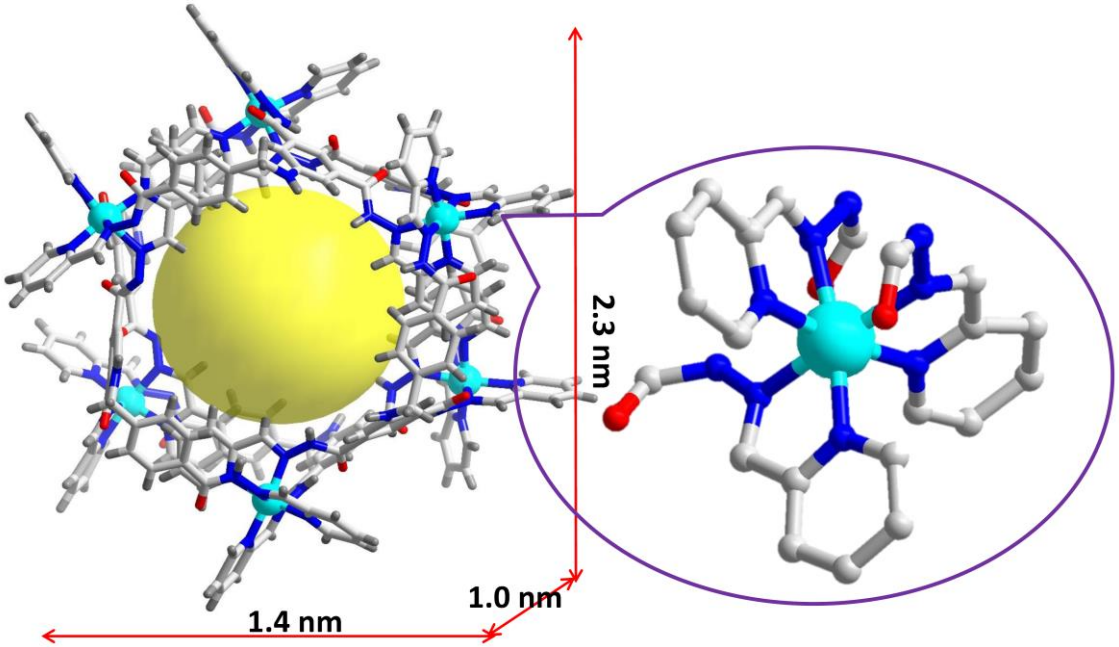

Figure S4 Coordination geometry of Ni–**ML**. Selective bond distances (Å) and angles (°): Ni(1)–N(1) 2.088(6), Ni(1)–N(2) 2.105(6), Ni(1)–N(3) 2.110(7), Ni(1)–N(4) 2.073(7), Ni(1)–N(5) 2.072(6), Ni(1)–N(6) 2.112(7), N(1)–Ni(1)–N(2) 79.3(2), N(3)–Ni(1)–N(4) 79.7(3), N(1)–Ni(1)–N(3) 87.7(2), N(4)–Ni(1)–N(6) 100.0(3), N(3)–Ni(1)–N(6) 178.8(2).

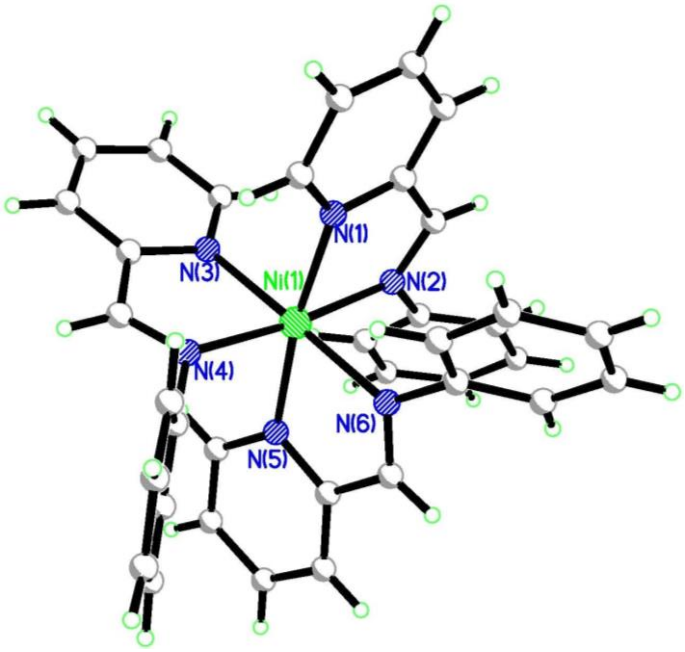

Figure S5 Simulation of the plausible encapsulation of anionic $Ru(dcbpy)_3$ into Ni–**YL** viewed along different directions by molecular force field-based calculations.

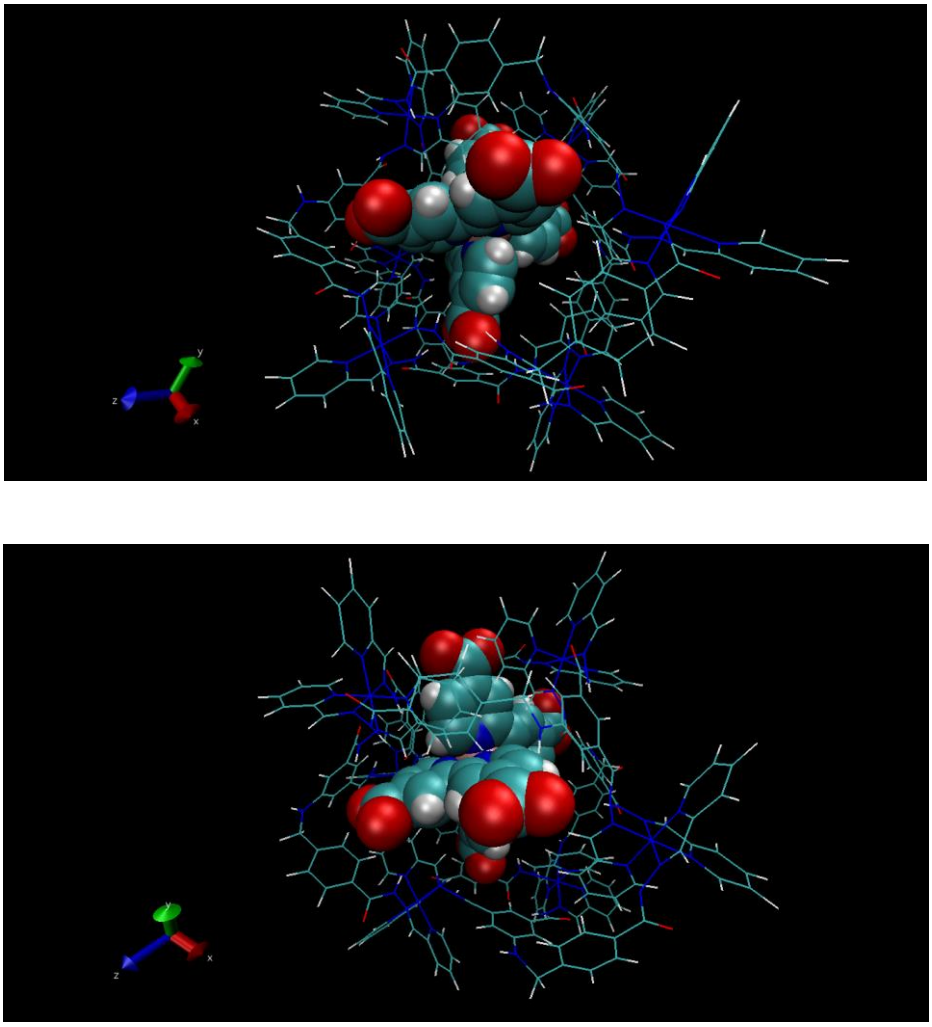

Figure S6 ESI-MS spectra of Ni–**YL** in acetonitrile (top) and upon addition of Ru(dcbpy)$_3$ (bottom).

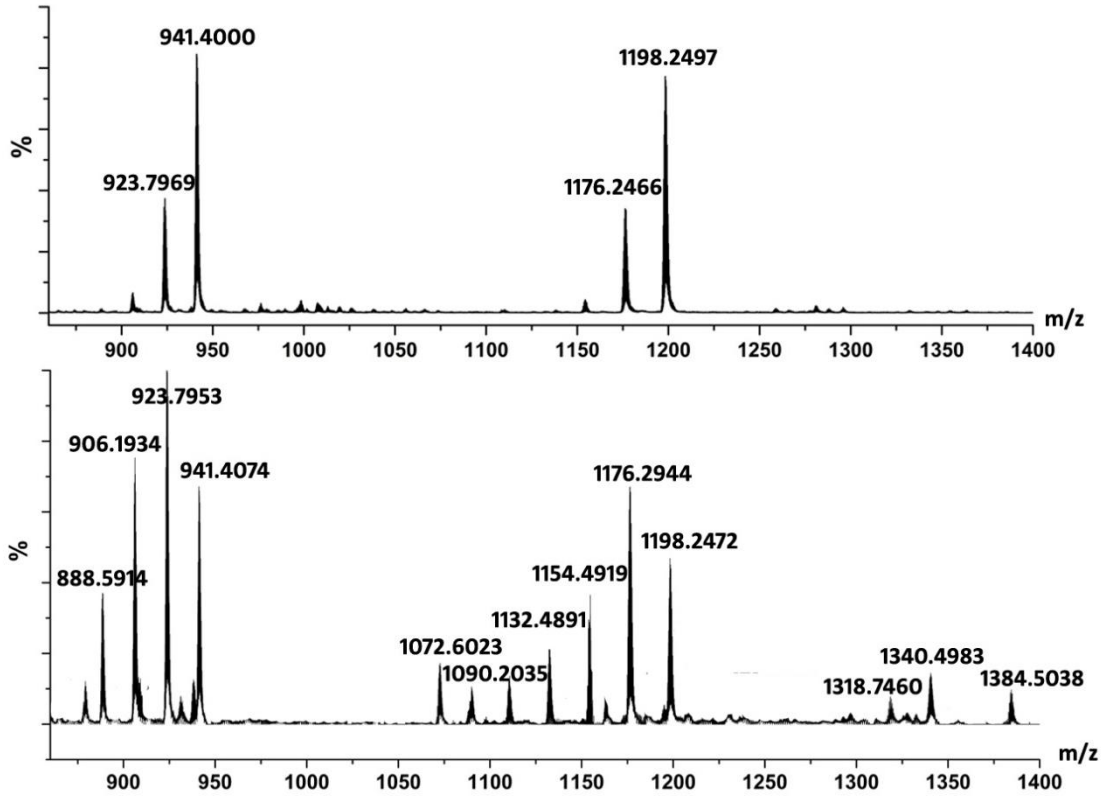

Peak number	Value	Charged	Species Assigned
1	888.5914	+5	[Ni$_6$**YL**$_6$·4(BF$_4$)-3H]
2	906.1934	+5	[Ni$_6$**YL**$_6$·5(BF$_4$)-2H]
3	923.7953	+5	[Ni$_6$**YL**$_6$·6(BF$_4$)-H]
4	941.4074	+5	[Ni$_6$**YL**$_6$·7(BF$_4$)]
5	1072.6023	+5	[Ni$_6$**YL**$_6$·Ru(dcbpy)$_3$·5(BF$_4$)-4H]
6	1090.2035	+5	[Ni$_6$**YL**$_6$·Ru(dcbpy)$_3$·6(BF$_4$)-3H]
7	1132.4891	+4	[Ni$_6$**YL**$_6$·5(BF$_4$)-3H]
8	1154.4919	+4	[Ni$_6$**YL**$_6$·6(BF$_4$)-2H]
9	1176.2472	+4	[Ni$_6$**YL**$_6$·7(BF$_4$)-H]
10	1198.2472	+4	[Ni$_6$**YL**$_6$·8(BF$_4$)]
11	1318.7460	+4	[Ni$_6$**YL**$_6$·Ru(dcbpy)$_3$·4(BF$_4$)-6H]
12	1340.4983	+4	[Ni$_6$**YL**$_6$·Ru(dcbpy)$_3$·5(BF$_4$)-5H]
13	1384.5038	+4	[Ni$_6$**YL**$_6$·Ru(dcbpy)$_3$·7(BF$_4$)-3H]

Figure S7 ESI-MS spectra of Ni–**ML** in acetonitrile.

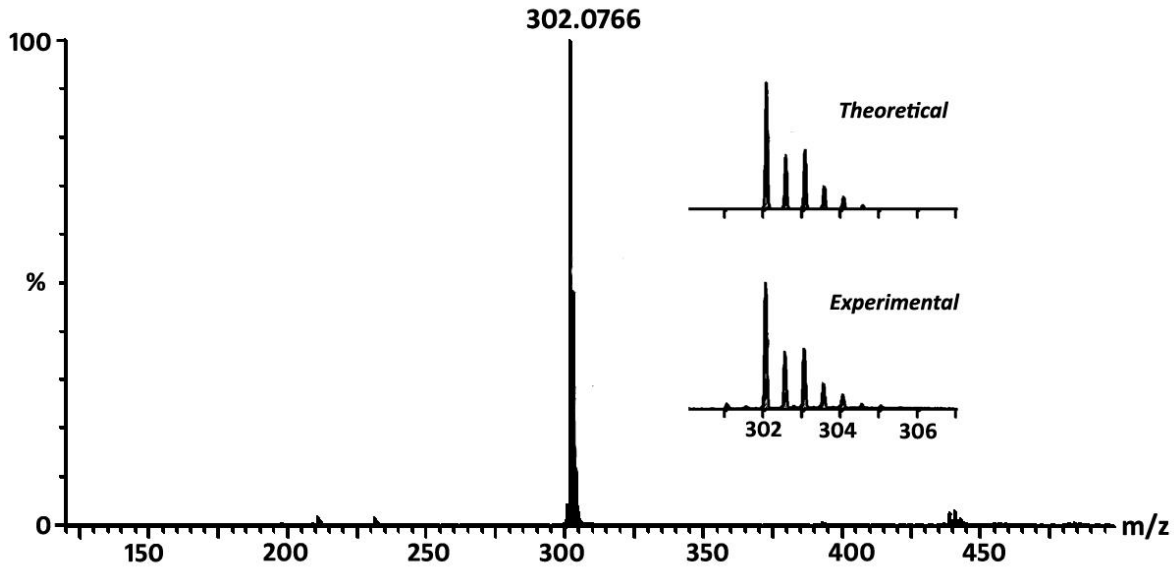

Peak number	Value	Charged	Species Assigned
1	302.0766	+2	Ni–**ML**

Figure S8 a) ^{1}H-NMR spectrum of Ru(dcbpy)$_3$ (0.1 mM) in the mixture of 1:1 D_2O and CD_3CN with a drop of NaOD; b) ^{1}H-NMR spectrum of Ru(dcbpy)$_3$ (0.1 mM) and Ni–**YL** (0.1 mM) in the mixture of 1:1 D_2O and CD_3CN; c) ^{1}H-NMR spectrum of Ni–**YL** in DMSO-d_6.

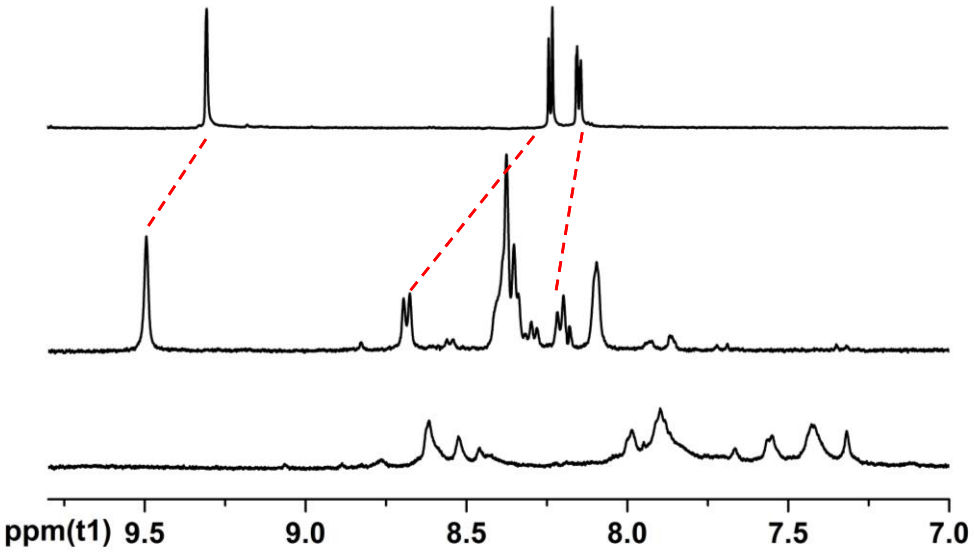

Figure S9 Hill-plot (right) of the emission quenching (left) of $Ru(dcbpy)_3$ (10 μM) by Ni–**YL** in 1:1 EtOH/H_2O at pH 10.5.

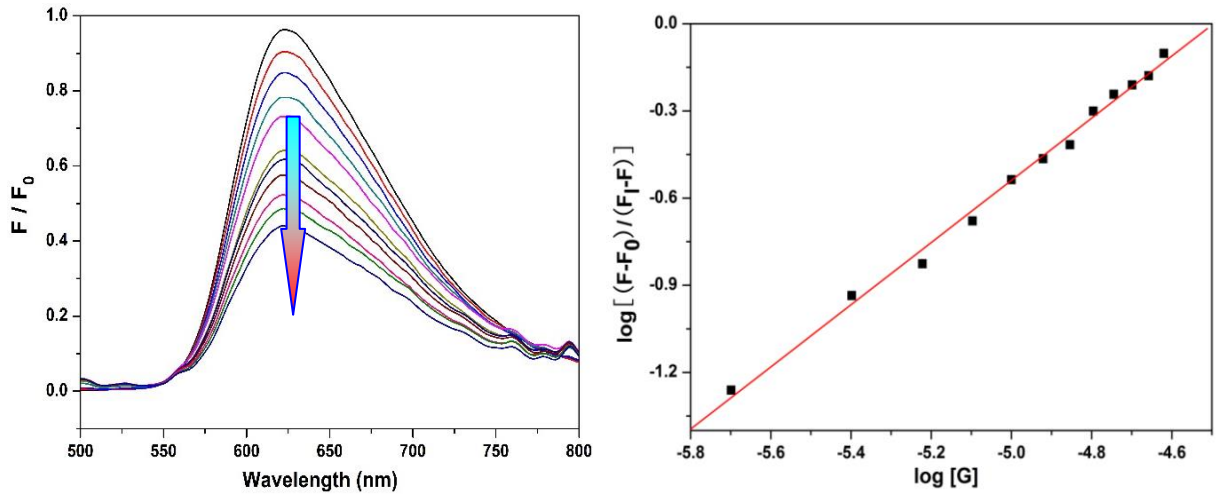

Figure S10 Stern-Volmer plot (right) of the emission quenching (left) of $Ru(dcbpy)_3$ (10 μM) by TEOA in 1:1 EtOH/H_2O at pH 10.5. (The best-fit equation of the Stern-Volmer plots indicated on the right)

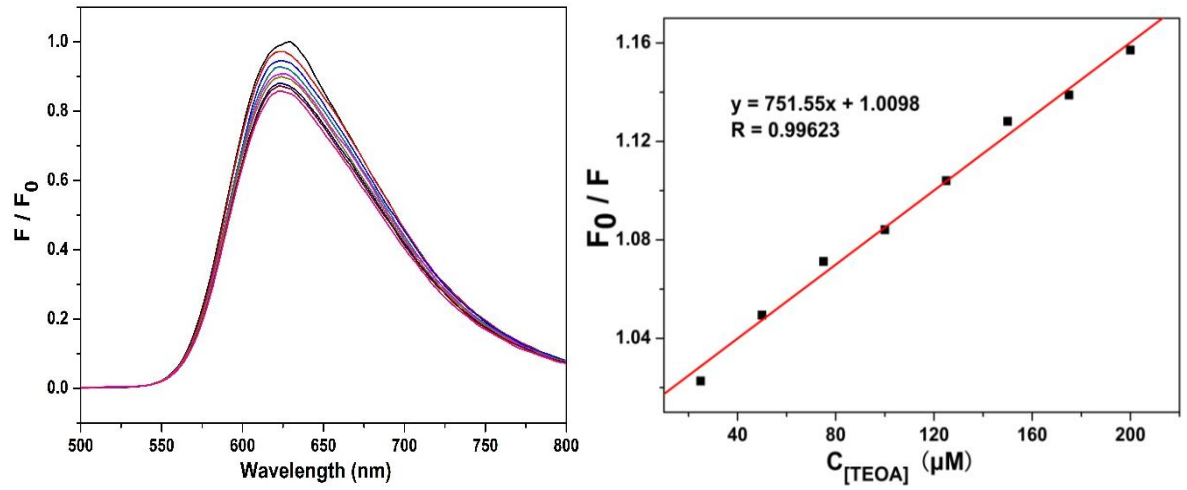

Figure S11 (a) Cyclic voltammograms of Ni–**ML** (1 mM) in a CH_3CN solution containing $TBAPF_6$ (0.1 M); (b) The addition of 2.0, 4.0, 6.0 and 8.0 ratio of TEOA·HCl in Ni–**ML** above solution. Scan rate: 100 mV/s.

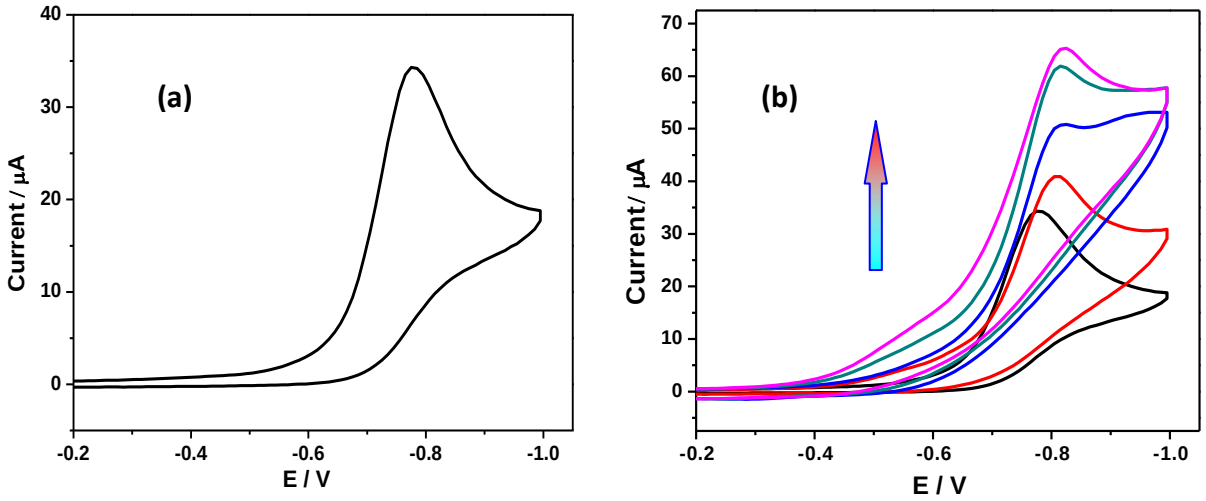

Figure S12 Stern-Volmer plot (right) of the emission quenching (left) of $Ru(dcbpy)_3$ (10 μM) by Ni–**ML** in 1:1 EtOH/H_2O at pH 10.5. (The best-fit equation of the Stern-Volmer plot is indicated on the right with the Stern-Volmer constant calculated as $1.95 \pm 0.13 \times 10^3\ M^{-1}$)

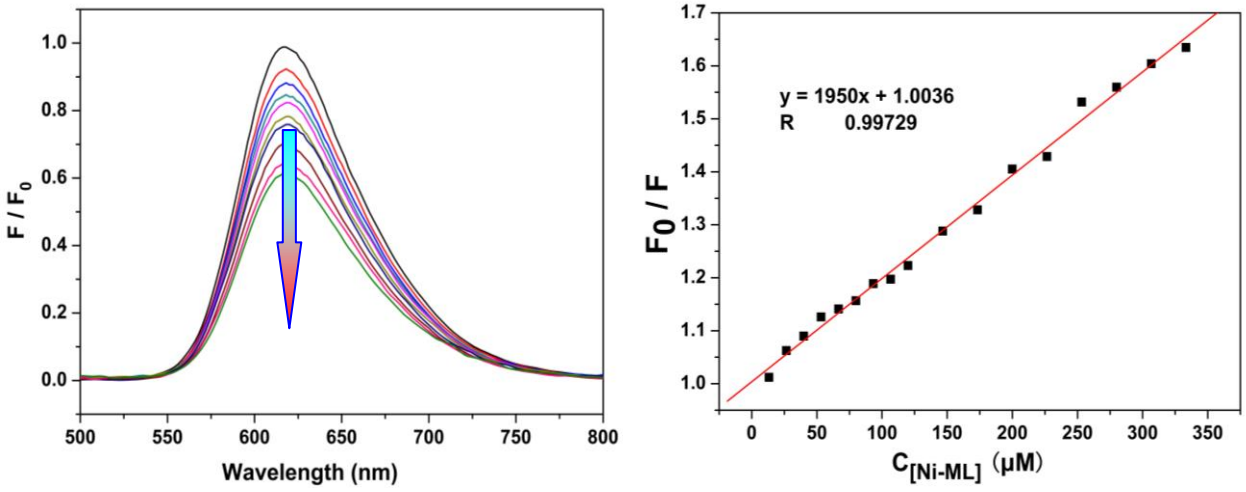

Figure S13 Fluorescence decay curves using 472.6 nm laser for resource at emission of 620 nm: (a) $Ru(dcbpy)_3$ (10 μM) in $EtOH/H_2O$= 1:1 at pH = 10.5; (b) the addition of 20 μM Ni–**YL**; (c) the addition of 0.12 mM Ni–**ML**.

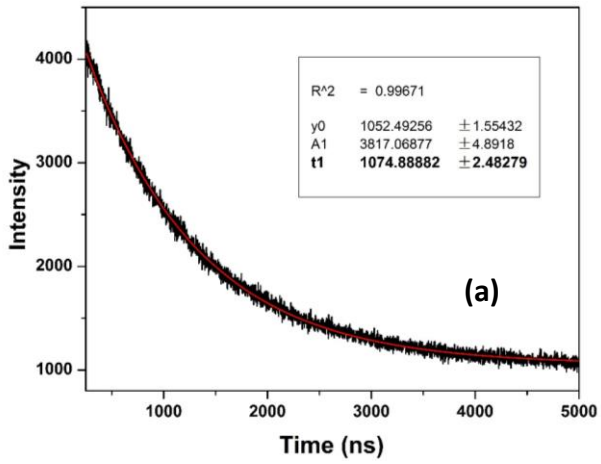

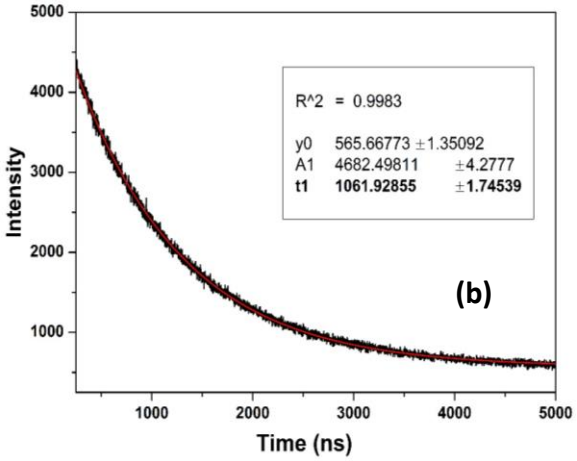

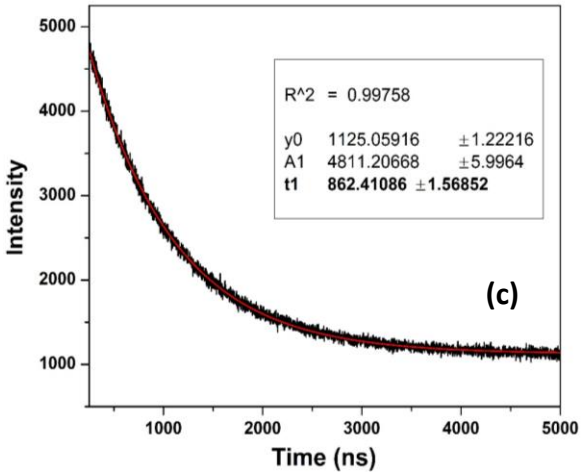

Figure S14 Fluorescence spectra of $Ru(dcbpy)_3$ (10 μM, black line) in $EtOH/H_2O$ (1:1, pH = 10.5) upon addition of Ni–**YL** (left, 50 μM, red line) or Ni–**ML** (right, 0.3 mM, red line) with $Fe(dcbpy)_3$ (left: 0.1 mM; right: 0.6 mM, blue line in both picture), respectively, showing the recovery of emission in the presence of $Fe(dcbpy)_3$, excited at 470 nm.

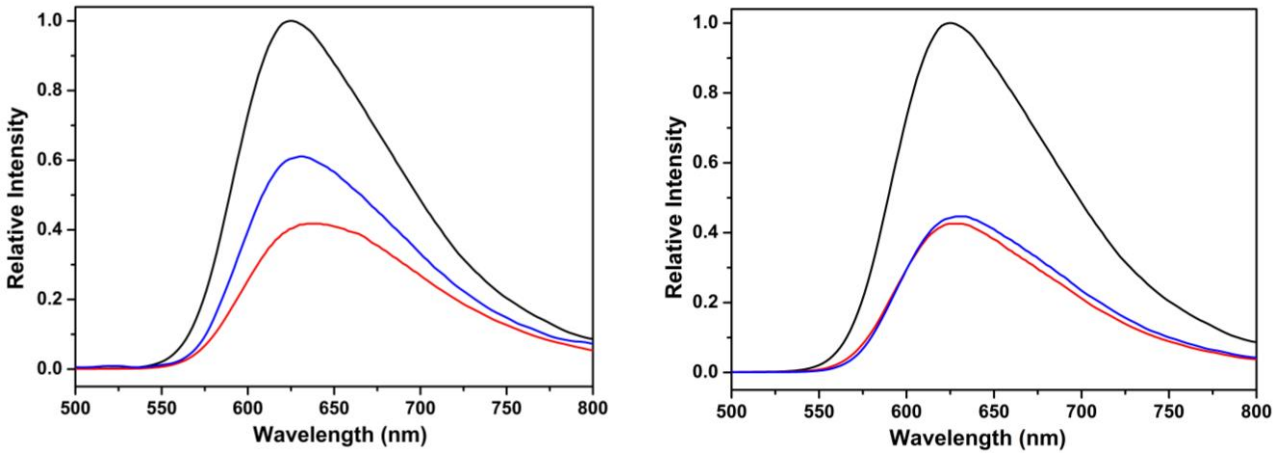

Figure S15 Left: Influence of the pH on photo-induced hydrogen production containing Ni–**YL** (10 μM), $Ru(dcbpy)_3$ (2.0 mM), TEOA 10 %, in $EtOH/H_2O$ = 1:1 in 5 h of irradiation; Right: Influence of the TEOA concentration on photoinduced hydrogen production containing Ni–**YL** (10 μM), $Ru(dcbpy)_3$ (2.0 mM), in $EtOH/H_2O$= 1:1 in 5 h of irradiation.

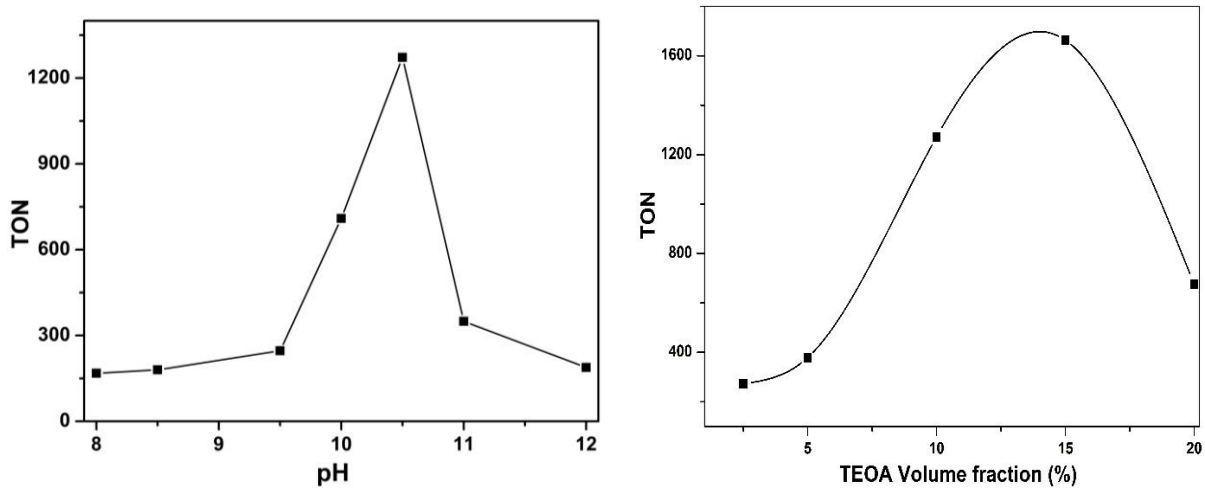

Figure S16 Transients absorption of spectra of $*Ru(dcbpy)_3$ with TEOA (15 %, red) in $EtOH/H_2O$ (1:1 in volume) solution at 298 K recorded at 15 μs after laser flash under an nitrogen atmosphere. The emerging peak at 520 nm is ascribed to the Ru(I) species.